INTERNATIONAL JOURNAL of RENEWABLE ENERGY RESEARCH
C. V. Rodriguez et al., Vol.16, No.2, June, 2026

# High-rise Building and Horizontal Axis Wind Turbine CFD Models Validation Using Two RANS Turbulence Models

Christian V. Rodriguez*‡, Alberto Ríos**, Jaime E. Luyo*

*Faculty of Mechanical Engineering, National University of Engineering, Lima, Peru

**Faculty of Systems, Electronics and Industrial Engineering, Technical University of Ambato, Ambato, Ecuador

(cvrodriguezd@uni.pe, a.rios@uta.edu.ec, jeluyo@yahoo.es)

‡Corresponding Author: Christian V. Rodriguez, Tel: +51 956 806671, cvrodriguezd@uni.pe

*Received: 23.02.2024 Accepted: 31.03.2024*

**Abstract-** Various Computational Fluid Dynamics (CFD) studies on high-rise buildings and horizontal axis wind turbines models have been conducted independently over the past decades. However, neither study has addressed the validation of results from both models within the same work. The primary objective of this study was to validate CFD simulations of a high-rise building and a horizontal axis wind turbine by employing the Realizable k-ε and SST k-ω turbulence models, aiming to determine the model that exhibits the highest accuracy when compared with experimental data available in the literature. Initially, models for the building and turbine were developed. Subsequently, grid independence studies were performed for both models. Finally, numerical results from both models were compared using validation metrics, including Hit Rate (HR), Normalized Mean Square Error (NMSE), and Mean Square Error (MSE). Overall, the Realizable k-ε model achieved superior results (NMSE = 0.022) compared to the SST k-ω model (NMSE = 0.039) in predicting the flow pattern on the building rooftop. Conversely, in simulations of the turbine, the SST k-ω (MSE = 0.370) outperformed the Realizable k-ε model (MSE = 0.445). These findings suggest that for CFD simulations of both models, particularly in urban wind energy applications, the SST k-ω model can be effectively employed.

**Keywords** Wind energy, Computational fluid dynamics, High-rise building, Horizontal axis wind turbine.

## 1. Introduction

Urban wind turbine technology is a field with great potential [1] to supply local electricity to residential and commercial buildings [2]. One of the key challenges within this field is attaining precise accuracy in Computational Fluid Dynamics (CFD) simulations of wind flows in urban environments and the resulting power outputs of wind turbines. It is important to note that accurately predicting urban wind patterns is crucial for the optimal micrositing of wind turbine, directly impacting the generated power output. Moreover, the computational resources required for simulating urban wind turbines present another important consideration. High-fidelity simulations require high computational resources, while low-accuracy CFD simulations can be executed with lower computational demands.

CFD model validation represents a critical stage in numerical simulations, as it determines the accuracy level exhibited by numerical results when compared with experimental measurements. In this work, validation processes were conducted for two CFD models: a high-rise building and a horizontal axis wind turbine.

CFD validation of urban environments encompasses the analysis of single buildings [3], around which wind flow analyses are required, or even larger groups of buildings [4], representing an area of interest. Previous CFD validations of different urban environments have been performed, as summarized in Table 1. For instance, Yoshie et al. [5] simulated a single high-rise building model (details provided in Table 1) and arrangements of buildings using Reynolds-Average Navier Stokes (RANS) and Large Eddy Simulation (LES) approaches. Vranešević et al. [6] evaluated wind speeds

around a prismatic 1:3 square building model through LES simulations. Their validation process involved comparing numerical results with experimental measurements via the Mean Normalized Bias (MNB) metric, reaching deviations below 6% and 18.5% for mean and fluctuating pressure coefficients (Cp), respectively. Additionally, Masoumi-Verki et al. [7] investigated the influence of different stratification conditions on wind flow and concentration fields around an isolated high-rise building. In their validation process, they considered metrics such as Hit Rate (HR) and Factor of two of observations (FAC2), achieving good quality numerical results (HR > 0.66 and FAC2 > 0.5).

The realistic modelling of large urban areas provides an ideal framework for analyzing urban wind flow dynamics. In this context, Juan et al. [8] conducted a numerical study on the wind energy potential around high-rise buildings within a realistic urbanized area (see Table 1). Their numerical results were subjected to validation against wind measurements. The CFD simulations utilized meshes comprising over 70'000 000 cells, requiring high computational resources available only on supercomputers. Additionally, Juan et al. [9] investigated the wind energy potential around four generic high-rise buildings using 3D RANS steady-state simulations. The simulations employed meshes containing 5'464 450 cells and incorporated various turbulence models including Standard k-ε, Realizable k-ε, RNG k-ε, SST k-ω and Reynolds Stress Model (RSM). Comparative analysis against wind tunnel measurements revealed that the RSM model exhibited the closest agreement with experimental mean velocities, achieving an average absolute deviation of 4%. However, in the present study, CFD simulations were limited to a high-rise building model due to constraints on computational resources.

As shown in Table 1, Tominaga et al. [10] conducted simulations of wind flow around a high-rise building using Unsteady Reynolds-Averaged Navier Stokes (URANS) k-ε turbulence models and LES. The high-rise building was according to Case A specifications outlined by the Architectural Institute of Japan [11]. Among the k-ε turbulence models, the MMK model provided the closest approximation of the dimensionless reattachment length ($X_L$) over the building rooftop (0.52, consistent with experimental value). Additionally, the Durbin model exhibited the closest agreement between numerical results and experimental measurements for wind velocities (U) and turbulent kinetic energy (k). Furthermore, Gousseau et al. [12] conducted a validation study of the same high-rise building, employing LES with two structured meshes containing 737 920 and 2'504 160 cells. The results demonstrated a good agreement for U, with HR ranging between 0.84 and 0.9, while HR values below 0.66 were computed for k. Liu and Niu [13] utilized steady RNG k-ε, LES and Detached Eddy Simulation (DES) modelling approaches to simulate the high-rise building. The simulations employed structured meshes containing between 1'280 000 and 9'250 000 cells. Their numerical results exhibited good agreement with experimental measurements across all approaches, achieving $X_L$ between 0.58 and 0.60. Note that the numerical results from DES and LES demonstrated better agreement with the experimental data compared to those obtained using RANS.

Regarding RANS simulations (Table 1), Tominaga [14] conducted a study comparing different k-ε based and k-ω based turbulence models in predicting wind flow around the high-rise building. Both steady and unsteady simulations were performed using the Fluent solver, with a mesh comprising 551 112 cells. The k-ε based simulations demonstrated better agreement with $X_L$ (0.60) compared to the k-ω based simulations (greater than 1) due to an overestimation of flow separation at building corners. Among the unsteady simulations, the RNG k-ε turbulence model with modified ε-equation showed the closest agreement with experimental measurements, achieving HR and Normalized Mean Square Error (NMSE) values of 0.67 and 0.37 for U and k, respectively. Toja-Silva et al. [15] also simulated the high-rise building using various steady-state RANS turbulence models implemented in OpenFOAM. The k-ε based and SST k-ω turbulence models, employing a mesh with 3'100 000 cells in the grid independence study, were tested by the authors. The Durbin-new model, proposed by the authors, exhibited the best agreement with experimental measurements for $X_L$ (0.52, similar to the experiment). Conversely, the Nonlinear Shih and SST k-ω models showed the worst results, both yielding values greater than 1 for $X_L$. Regarding U and k, the RNG, MMK, Durbin, Yap and Nonlinear Shih models successfully passed validation, achieving HR values greater than 0.813 and 0.688, respectively. Furthermore, Shirzadi et al. [16] optimized four closure coefficients of the Kato and Launder k-ε turbulence model for steady wind flow around the high-rise building using stochastic optimization and Monte Carlo sampling techniques. Their simulation, conducted with Ansys CFX and a mesh containing 396 864 cells, demonstrated that the optimization of closure coefficients led to improvements in HR and FAC2 for U from 0.31 and 0.54 to 0.47 and 0.91, respectively.

Note that all the studies mentioned utilized structured meshes with rectangular domains, as outlined in Table 1, with the exception of Xiong et al. [17], who employed polyhedral mesh elements. Xiong et al. [17] conducted CFD simulations of airflow around the high-rise building using different polyhedral meshes and k-ε turbulence models. The authors also conducted a validation process, comparing numerical predictions with experimental measurements, employing the Error Rate (ER) metric. The results showed ER lower than 16% for the simulated cases. For additional details regarding the aforementioned studies, refer to Table 1.

Regarding horizontal axis wind turbines (Table 2), Sorensen et al. [18] conducted simulations on the two-bladed 10 m diameter Phase VI rotor from NREL. They simulated only one blade using the EllipSys3D solver with the SST k-ω turbulence model. Steady and unsteady simulations were carried out using two structured meshes containing 3'100 000 and 4'200 000 cells. The computational domains were characterized by circular and cylindrical topologies. Overall, the numerical results showed good agreement with the measurements, with a maximum deviation of 20% observed for the low-speed shaft torque at U = 10 m/s.

**Table 1.** Numerical validation studies of high-rise buildings

| Author | Building | Software | Approach | Turbulence model | Max mesh cells | Parameter | Metric |
|---|---|---|---|---|---|---|---|
| Yoshie et al. [5] | High-rise building | - | RANS | Standard k-ε, Launder-Kato k-ε and RNG k-ε | 105 300 | $X_L$ and U | D |
| Juan et al. [8] | Large urban area | Fluent | RANS | Standard k-ε, Realizable k-ε and RNG k-ε | 71’109 937 | TI and U | D |
| Juan et al. [9] | Four generic high-rise buildings | Fluent | RANS | Standard k-ε, Realizable k-ε, RNG k-ε, SST k-ω and RSM | 5’464 450 | TI and U | D |
| Masoumi-Verki et al. [7] | High-rise building | - | Embedded LES | - | 2’148 192 | k and U | HR and FAC2 |
| Vranešević et al. [6] | Prismatic square building | OpenFOAM | LES | - | 27’000 000 | Cp, TI and U | D and MNB |
| Xiong et al. [17] | High-rise building | CCM+ | RANS | Standard k-ε, Realizable k-ε, Abe–Kondoh–Nagano Low-Re k-ε, Elliptic Blending k-ε and V2F Low-Re k-ε | - | $X_L$, k and U | ER |
| Tominaga et al. [10] | High-rise building | - | URANS / LES | Standard k-ε, Launder-Kato k-ε, Modified Launder-Kato k-ε, MMK k-ε and Durbin k-ε | 105 300 | $X_L$, k and U | - |
| Gousseau et al. [12] | High-rise building | Fluent | LES | - | 2’504 160 | $X_L$, k and U | HR, FAC2, FB and NMSE |
| Liu and Niu [13] | High-rise building | Fluent | RANS / DES / LES | RNG k-ε | 9’250 000 | $X_L$ and U | - |
| Tominaga [14] | High-rise building | Fluent | RANS / URANS | Standard k-ε, Realizable k-ε, RNG k-ε, Standard k-ω and SST k-ω | 551 112 | $X_L$, k and U | HR, FAC2, FB and NMSE |
| Toja-Silva et al. [15] | High-rise building | OpenFOAM | RANS | Standard k-ε, RNG k-ε, MMK k-ε, Durbin k-ε, Durbin-Tominaga k-ε, Durbin-New k-ε, Yap k-ε, Nonlinear Shih k-ε and SST k-ω | 3’100 000 | $X_L$, k and U | HR |
| Shirzadi et al. [16] | High-rise building | CFX | RANS | Standard k-ε | 396 864 | $X_L$, T, k and U | HR and FAC2 |

Cp = Pressure coefficient; D = Deviation; ER = Error rate; FAC2 = Factor of two of observations; FB = Fractional bias; HR = Hit rate; k = Turbulent kinetic energy; MNB = Mean normalized bias; NMSE = Normalized mean square error; T = Temperature; TI = Turbulent intensity; U = Wind speed; $X_L$ = Dimensionless reattachment length.

Similarly, Kamalov et al. [19] investigated the aerodynamics of the Phase VI wind turbine blade employing an arbitrary hybrid turbulence model implemented in OpenFOAM. The authors compared this model to RANS-based transient simulations and validated the numerical model, achieving deviations lower than 4.2% between

numerical results and experimental measurements of torque. The simulations were conducted using a mesh comprising 54'937 248 cells for U = 15 m/s and a rotational velocity (ẇ) of 72 RPM. The arbitrary hybrid turbulence model demonstrated better results compared to RANS-based models, with errors of 10.2% and 16.5%, respectively.

The Phase VI wind turbine blade was integrated with a morphing trailing edge to increase its performance by Akhter et al. [20]. The study included a validation stage where numerical results were compared to experimental measurements of power coefficients ($C_P$). Transient simulations were conducted using the SST k-ω turbulence model with a mesh of 11'000 000 cells (refer to Table 2). The predictions for torque, including U between 5 and 13 m/s, yielded relative errors lower than 5.5%. Elfarra et al. [21] optimized a winglet for the Phase VI wind turbine rotor from NREL, which was employed in a validation process through steady-state simulations using the Fine/Turbo NUMECA solver with the k-ε Launder-Sharma turbulence model. U ranging from 5 to 25 m/s were considered, and a structured mesh with 350 000 nodes was generated for the simulations. The validation results demonstrated good agreement with experimental power data in the low and mid U regions. Similarly, Abdelghany et al. [22] enhanced the aerodynamic characteristics of a horizontal axis wind turbine blade by adding a winglet at its tip, using NACA 4418 airfoils. Validation processes comparing $C_P$ measurements with numerical results were conducted. The CFD simulations employed the SST k-ω and Spalart-Allmaras turbulence models, yielding maximum errors of 2% and 10%, respectively. Based on these findings, the authors concluded that the SST k-ω model was most suitable for simulating airflow around the wind turbine blade. Abdelsalam and Ramalingam [23] studied the wake behavior of the Danwin 180 kW wind turbine using the Standard k-ε turbulence model. Steady-state simulations were performed with an unstructured mesh containing 2'900 000 cells. The results showed good agreement with experimental data, leading the authors to conclude that the Standard k-ε could accurately predict wake behavior when the rotor was precisely modeled.

The wake behind the three-bladed 4.5 m diameter MEXICO wind turbine [24] was investigated by Bechmann et al. [25], as detailed in Table 2. They conducted steady-state simulations using U ranging from 10 to 24 m/s with the SST k-ω turbulence model implemented in the EllipSys3D solver. A structured mesh containing 16'000 000 points was utilized for the simulations. The MEXICO wind turbine rotor was also investigated by Regodeseves and Morros [26], employing a structured mesh containing 37'500 000 cells. They utilized both k-ε based and SST k-ω turbulence models to solve URANS equations in Fluent. Simulations were conducted for three wind speeds (10, 15 and 24 m/s), considering the turbine geometry including the rotor, nacelle and tower. Similarly, Rodrigues and Lengsfeld [27] validated CFD simulations of the MEXICO wind turbine employing the SST k-ω turbulence model and Moving Reference Frame (MRF) technique for U of 10 and 15 m/s. Steady-state simulations were performed using unstructured meshes containing between 2'000 000 and 10'000 000 cells. The numerical results from these studies exhibited good agreement with experimental measurements.

Herraez et al. [28] further validated the numerical results of the MEXICO wind turbine using the Spalart-Allmaras turbulence model in OpenFOAM. They conducted steady and unsteady CFD simulations with U of 10, 15 and 24 m/s, and ẇ of 424.4 RPM. A structured mesh comprising 11'000 000 cells was utilized for the simulations. The numerical results demonstrated reasonable agreement with experimental measurements. Similarly, Amini et al. [29] simulated the MEXICO turbine using the same wind speeds and employing the Spalart-Allmaras model in OpenFOAM. They also utilized a structured mesh and achieved good agreement between numerical results and experimental data. Furthermore, Rocha et al. [30] investigated the calibration of the SST k-ω turbulence model by simulating two small wind turbines using OpenFOAM. The wind turbine blades were modelled with NACA 0012 and NACA 4412 airfoils. Steady-state simulations were conducted with structured meshes containing between 1'600 000 and 3'200 000 cells. Additional details can be seen in Table 2.

Regarding buildings and wind turbines simulations conducted in the same work, Larin et al. [31] investigated the performance of a Savonius wind turbine positioned near the upstream edge of a building. They validated the turbine CFD simulations with experimental data using the Realizable k-ε, Spalart-Allmaras and SST k-ω turbulence models in Fluent. The authors conducted unsteady 3D simulations of both the building and the turbine using the Realizable k-ε model. This turbulence model was selected based on its superior agreement with experimental measurements during the 2D validation stage of the turbine, exhibiting an average overprediction of $C_P$ by 20%. In the validation of the 3D building model, the authors calculated maximum errors of 7.3%. Similarly, Krishnan and Paraschivoiu [32] investigated the performance of a diffuser-shaped shroud located on a building rooftop. The authors performed unsteady 3D simulations of both the building and a Savonius turbine using the Realizable k-ε turbulence model. The simulations utilized an unstructured mesh containing about 6'000 000 cells. Additionally, Arteaga-Lopez et al. [2] proposed a methodology to assess the placement of urban wind turbines. Initially, the authors simulated an urban environment to identify a target building with high wind velocities around it. Various Bergey Excel horizontal axis wind turbines were then placed and analyzed on the target building. The CFD simulations were conducted using SolidWorks Flow Simulation software with the k-ε turbulence model. A structured mesh containing 176 260 cells was employed in the simulations. While the authors mentioned a successful validation process of the Bergey Excel wind turbine numerical results, they did not provide these results.

It's noted that previous CFD studies have separately validated high-rise building and horizontal axis wind turbine models, but neither study shown the validation of both models' CFD results in the same work. However, in the present work, both models, based on Case A of the Architectural Institute of Japan and the MEXICO project, respectively, are being validated.

**Table 2.** Numerical validation studies of horizontal axis wind turbines

| Author | Turbine | Software | Approach | Turbulence model | Domain | Mesh type | Max mesh cells | Parameter | Metric |
|---|---|---|---|---|---|---|---|---|---|
| Sorensen et al. [18] | Phase VI rotor | EllipSys3D | RANS / URANS | SST k-ω | C and CY | S | 4'200 000 | Cp, Cn, Ct, root flap moment, root edge moment and torque | D |
| Elfarra et al. [21] | Phase VI rotor | Fine/Turbo NUMECA | RANS | Launder-Sharma k-ε | CY | S | 350 000 (nodes) | Cp, Cn, Ct and power | - |
| Abdelsalam and Ramalingam [23] | Danwin 180 kW | Fluent | RANS | Standard k-ε | R | UST | 2'900 000 | U | - |
| Bechmann et al. [25] | MEXICO | EllipSys3D | RANS | SST k-ω | C | S | 16'000 000 (nodes) | Cp, Cn, thrust, U | D |
| Regodeseves and Morros [26] | MEXICO | Fluent | URANS | SST k-ω | R | S | 37'500 000 | Cp, Fn, Ft, thrust, torque, U | D |
| Rodrigues and Lengsfeld [27] | MEXICO | Fluent | RANS | SST k-ω | R | UST | 10'000 000 | Cp, Fn, Ft and U | - |
| Herraez et al. [28] | MEXICO | OpenFOAM | RANS / URANS | Spalart-Allmaras | CY | S | 11'000 000 | Cp and U | - |
| Amini et al. [29] | MEXICO | OpenFOAM | RANS | Spalart-Allmaras | R | S | - | Fn, Ft, U | - |
| Rocha et al. [30] | Two small wind turbines | OpenFoam | RANS | SST k-ω | CY | S | 3'200 000 | $C_P$ | RMSE |
| Abdelghany et al. [22] | Blades created using NACA 4418 airfoil | Fluent | RANS | SST k-ω and Spalart-Allmaras | CY | UST | 3'000 000 | $C_P$ | D |
| Akhter et al. [20] | Phase VI | Fluent | URANS | SST k-ω | CY | S | 11'000 000 | $C_P$ | D |
| Kamalov et al. [19] | Phase VI | OpenFOAM | URANS / LES | SST k-ω and arbitrary hybrid (VLES) | CY | S | 54'937 248 | Cp and torque | D |

C = Circular; CY = Cylindrical; Cn = Normal force coefficient; Ct = Tangential force coefficient; $C_P$ = Power coefficient; Cp = Pressure coefficient; D = Deviation; Fn = Normal force; Ft = Tangential force; R = Rectangular; RMSE = Root mean square error; ST = Structured; U = Wind speed; UST = Unstructured.

In the present work, RANS simulations are employed due to their lower computational cost compared to LES, even though RANS is less accurate. LES exhibits certain limitations. One such limitation is its requirement for a high-resolution grid to effectively capture the flow dynamics around structures like buildings, streets, and the turbine itself. Additionally, accurate boundary conditions are essential for representing the interactions between the flow and the urban environment in LES simulations. Furthermore, LES is susceptible to numerical stability issues, particularly in scenarios involving highly intricate geometries and flow conditions. To address this, subgrid models are employed in LES to account for the effects of smaller eddies that are not resolved by the grid. However, these subgrid models introduce uncertainties that can impact the accuracy of simulation results, especially in complex urban settings where flow patterns are heavily influenced by building morphology and terrain characteristics. RANS simulations, despite their drawbacks in capturing all turbulence scales, especially in complex turbulent flows or near walls, and in predicting flow separation, reverse flow, and unsteady flow phenomena compared to LES, still provide reasonable results. Additionally, steady-state simulations are chosen over unsteady-state ones due to limited computational resources. While unsteady simulations typically yield better agreement with experimental measurements, steady simulations require fewer computational resources. Furthermore, structured meshes are utilized in this work because they require fewer cells compared to unstructured meshes while still achieving accurate results. This approach helps optimize computational efficiency without compromising accuracy (see Table 1 and Table 2).

Broadly, k-ε linear eddy viscosity models have been utilized for simulations of both buildings and wind turbines. Within urban environment modelling, k-ε turbulence models have shown good agreement with measurements [4][13][14], while the SST k-ω model has presented difficulties, particularly in capturing wind flow reattachment lengths on building rooftops [15]. However, the SST k-ω turbulence model has demonstrated better agreement than the standard k-ε for modelling horizontal axis wind turbines [18][21][23][25][27]. The y+ dimensionless parameter plays a crucial role in predicting proper wind flow behavior around surfaces, particularly in capturing boundary layer physics. For the SST k-ω turbulence model, y+ values below 5 are maintained on the blade surface, while for k-ε based turbulence models, y+ values between 30 and 300 are typically used, or even less than 5 when employing the enhanced wall treatment. This makes the SST k-ω model more computationally demanding. It's important to note that the selection of turbulence models involves a trade-off between precision and computational cost [15], making it challenging to find a numerical model that excels in resolving all cases involving different physical phenomena [33]. In the present work, CFD simulations of both the high-rise building and horizontal axis wind turbine are conducted using the Realizable k-ε [34] with enhanced wall treatment and SST k-ω [35] turbulence models.

Accordingly, the main objective of this work is to compare the Realizable k-ε and SST k-ω turbulence models through the numerical validation of the CFD simulation results of a high-rise building and a horizontal axis wind turbine to determine which model demonstrates the best accuracy using comparative metrics such as HR, NMSE and MSE. The methodology to be employed in this work is outlined in Figure 1. Firstly, detailed models of the high-rise building and the horizontal axis wind turbine are provided, along with the CFD numerical configurations utilized in the simulations. Next, grid independence studies are conducted to identify meshes that yield results independent of grid resolution. These meshes are then utilized in subsequent simulations. Subsequently, the predictions obtained with the models of the high-rise building and the horizontal axis wind turbine are compared with experimental measurements from the literature using comparative metrics. Finally, based on the results, a discussion is conducted to highlight the main findings.

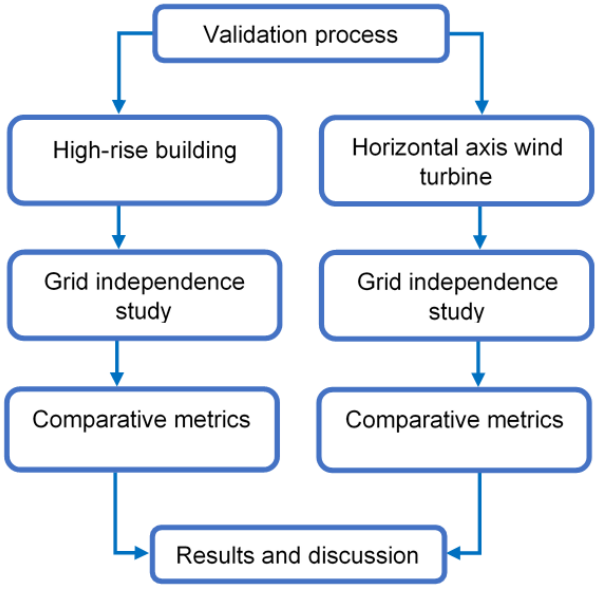


**Fig. 1.** Methodology used in this work.

Thus, the methods used in this work are detailed in Section 2. Section 3 shows the results of this study and the main discussion related to them. Finally, the conclusions are presented in Section 4.

## 2. Methods

The RANS formulation for steady-state, incompressible flow of Newtonian fluid can be expressed as follows [36],

$$\frac{\partial \bar{u}_i}{\partial x_i} = 0, \tag{1}$$

$$\frac{\partial (\bar{u}_i \bar{u}_j)}{\partial x_j} = -\frac{1}{\rho}\frac{\partial \bar{p}}{\partial x_i} + \frac{\partial}{\partial x_j}\left(\mu \frac{\partial \bar{u}_i}{\partial x_j} - \overline{u_i' u_j'}\right), \tag{2}$$

for the mass and momentum conservation, respectively. $\bar{u}_i$ and $u_i'$ are the mean and fluctuating velocities, $\bar{p}$ represents the average pressure, and ρ and μ are the density and kinematic viscosity, respectively. To deal with the Reynolds stresses $\overline{u_i' u_j'}$ that appear in the RANS formulation, the Realizable k-ε and SST k-ω turbulence models are employed in this work.

The transport equations of the Realizable k-ε turbulence model in steady-state [34] for the turbulent kinetic energy (k) and turbulence dissipation rate (ε), respectively, are as follows,

$$\frac{\partial(\rho\bar{u}_j k)}{\partial x_j} = \frac{\partial}{\partial x_j}\left[\left(\mu + \frac{\mu_t}{\sigma_k}\right)\frac{\partial k}{\partial x_j}\right] + P_k - \rho\varepsilon - Y_M, \quad (3)$$

$$\frac{\partial(\rho\bar{u}_j \varepsilon)}{\partial x_j} = \frac{\partial}{\partial x_j}\left[\left(\mu + \frac{\mu_t}{\sigma_\varepsilon}\right)\frac{\partial \varepsilon}{\partial x_j}\right] + C_{\varepsilon 1}P_b\frac{\varepsilon}{k}C_{\varepsilon 3} - \rho C_{\varepsilon 2}\frac{\varepsilon^2}{k+\sqrt{\nu\varepsilon}}, \quad (4)$$

where $\mu_t$ represents the turbulent viscosity and $P_k$ is the production of k. $P_b$ is the generation of k due to buoyancy. $Y_M$ represents the contribution of the fluctuating dilation to the overall dissipation rate. $\sigma_k$, $\sigma_\varepsilon$, $C_{\varepsilon 1}$ and $C_{\varepsilon 2}$ are the closure coefficients which balance the turbulence model equations. These closure coefficients are generally calibrated using experiments, empirical correlations or numerical simulations. Although optimum values for these coefficients have been obtained in previous studies for the high-rise building [16] and horizontal axis wind turbine [30] models, this study utilizes the standard values of these coefficients provided in the Fluent solver.

The steady-state transport equations of the SST k-ω turbulence model [35] are,

$$\frac{\partial(\rho\bar{u}_j k)}{\partial x_j} = \frac{\partial}{\partial x_j}\left[\Gamma_k\frac{\partial k}{\partial x_j}\right] + \bar{P}_k - Y_k, \quad (5)$$

$$\frac{\partial(\rho\bar{u}_j \omega)}{\partial x_j} = \frac{\partial}{\partial x_j}\left[\Gamma_\omega\frac{\partial \omega}{\partial x_j}\right] + P_\omega - Y_\omega + D_\omega, \quad (6)$$

for k and the specific dissipation rate (ω), respectively. $\Gamma_k$ and $\Gamma_\omega$ are the effective diffusivity of k and ω. $\bar{P}_k$ and $P_\omega$ are the generation of k due to mean velocity gradients and the generation of ω, respectively. $Y_k$ and $Y_\omega$ represent the dissipation of k and ω. $D_\omega$ is the cross-diffusion term.

The SIMPLE algorithm is utilized to solve the partial differential equations, while the least squares cell-based method is employed for gradient evaluation. The second-order scheme is applied for pressure, and the second-order upwind scheme is utilized for momentum, k, ε and ω. The convergence criterion in the simulations is set with residuals of $10^{-5}$ for all variables. ICEM CFD and Fluent software are employed for mesh generation and numerical simulations, respectively.

### *2.1. High-Rise Building*

#### *2.1.1. Grid independence study*

The case study to validate the numerical model predicting the wind flow around a high-rise building follows the specifications of Case A outlined by the Architectural Institute of Japan [11]. Detailed experiment characteristics and wind tunnel data for Case A can be found in reference [37]. The geometry of the high-rise building, with b of 0.08 m, is depicted in Figure 2.

The computational domain, which represents the wind tunnel, is illustrated in Figure 3. It has dimensions of 1.72, 1.1 and 0.9 m in x, y and z directions, respectively. The upstream face of the building is located 0.4 m from the Inlet. Different profiles are imposed at the Inlet. The Ground, Building and Sky surfaces are treated as walls, while the Front and Back faces are designated as symmetry planes. The Outlet boundary is assumed to be a pressure outlet.

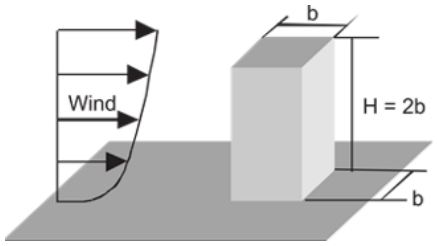


**Fig. 2.** Single high-rise building [5].

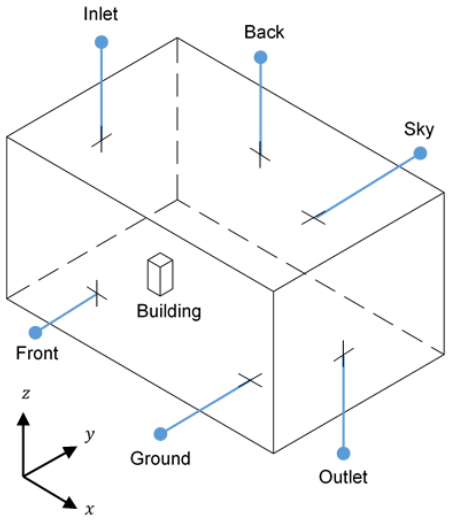


**Fig. 3.** Computational domain of the high-rise building.

The profiles of U, k and ε imposed at Inlet surface for the building simulation validation are shown in **Figure 4**. It's worth noting that the boundary conditions used here are according to the specifications outlined by the Architectural Institute of Japan [11] and Tominaga et al. [10].

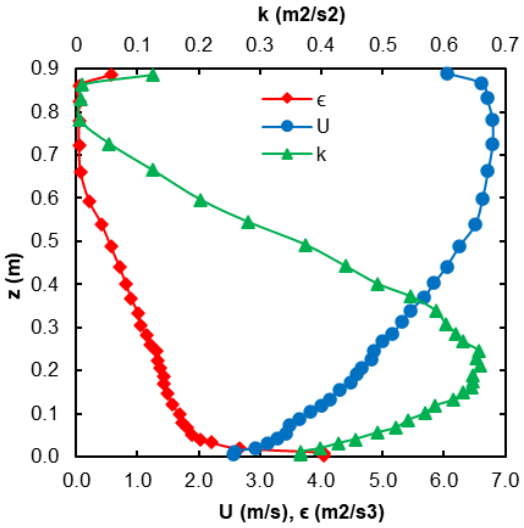


**Fig. 4.** Inlet profiles of U, k and ε [15][37].

For the grid independence study, two meshes are constructed: a coarse mesh containing 3'008 362 cells and a fine mesh with 14'371 790 cells. Growth rates of 1.2 and 1.1 are employed for the Coarse and Fine meshes, respectively. The y+ values on the walls of the meshes are kept below 5, as recommended for k-ε based turbulence models with enhanced wall treatment approach and the SST k-ω model. Note that the enhanced wall treatment used here combines the two-layer model with enhanced wall functions, similar to that implemented in Ansys Fluent. The Realizable k-ε model is employed in the grid independence study. Numerical results of U and k are compared at specific locations V2 (x = 0.40 m), V3 (x = 0.42 m), V4 (x = 0.44 m) and V5 (x = 0.48 m) on the building rooftop (see Figure 5).

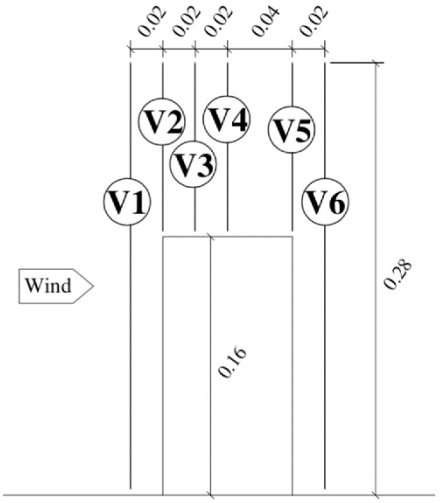


**Fig. 5.** Vertical axes for comparison of U and k results around the building [15].

### 2.1.2. Comparative metrics

In the grid independence study, the selected mesh is utilized to compared the results obtained using the Realizable k-ε and SST k-ω models result, via the HR and NMSE metrics. These metrics are calculated at positions V2 – V5 (see Figure 5). The HR metric indicates the level of success in predicting certain quantities (such as U and k), while NMSE quantifies the scatter of data (further details can be found in reference [38]). For an ideal model prediction, the HR metric would be 1, and the NMSE would be 0. The metrics are defined as follows,

$$HR = \frac{1}{N}\sum_{i=1}^{N} n_i \text{ with } n_i = \begin{cases} 1 \text{ for } \left|\frac{P_i - O_i}{P_i}\right| \le D_b \text{ or } |P_i - O_i| \le W_b, \\ 0 \text{ else} \end{cases} \quad (7)$$

$$NMSE = \frac{1}{N\,\bar{P}\,\bar{O}}\sum_{i=1}^{N}(P_i - O_i)^2, \quad (8)$$

where N is the number of data points, $P_i$ and $O_i$ represent the measured and predicted values for the ith sample. $\bar{P}$ and $\bar{O}$ are the averaged values, while $D_b$ and $W_b$ denote the threshold limits for HR. In this work, $D_b$ and $W_b$ are set to 0.25 and 0.03 for U, and 0.25 and 0.003 for k, consistent with the approach used by Gousseau et al. [12].

The HR represents the proportion of model outcomes that fall within an acceptable range, either $D_b$ or $W_b$, compared to the reference data. $D_b$ considers the relative uncertainty of the reference data, while $W_b$ characterizes the consistency or repeatability of the reference data [38]. On the other hand, NMSE is greatly affected by rare instances of high observations and corresponding predictions for the concentrations [38].

## 2.2. Horizontal Axis Wind Turbine

### 2.2.1. Grid independence study

The validation of the wind turbine model results is conducted using data from the MEXICO project (Model Experiments in Controlled Conditions), which was carried out in the Large-Scale Low Speed Facility of the German Dutch Wind Tunnel Organization [24]. The wind turbine features three blades with a rotor diameter (D) of 4.5 m and generates 7.6 kW mechanical power at U = 12 m/s. Its design is based on DU 91-W2-250, RISØ A1-21 and NACA 64-418 airfoils, as illustrated in **Figure 6**.

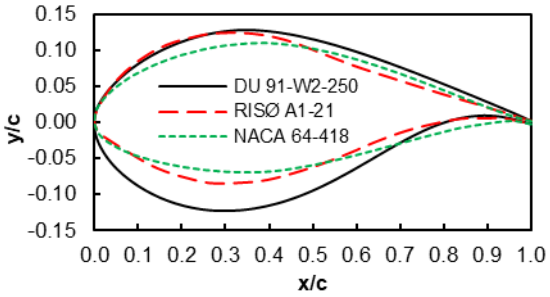


**Fig. 6.** Geometry of DU 91-W2-250, RISØ A1-21 and NACA 64-418 airfoils.

Detailed information regarding the chords, airfoil types, twist angles (β) and section pitch angles (θ) characterizing the MEXICO wind turbine blades is provided in Table 3. Note that the tip pitch angle is set to -2.3° and the rotor speed (ẇ) is 424.5 RPM. Three wind speeds, 10, 15 and 24 m/s, are simulated in this study. Additionally, it should be mentioned that the hub, nacelle and tower are not considered in the wind turbine modelling.

To account for periodicity, only one-third of the computational domain is simulated, as outlined in Figure 7. To address the rotational behavior of the wind turbine rotor, the MRF approach is employed. This approach considers the rotational effects on steady-state flows by incorporating centrifugal and centripetal forces into the governing equations of fluid dynamics [1]. For the simulations of the MEXICO wind turbine, two domains are required: the rotational domain, which contains the wind turbine, and the stationary domain, which situated farther from the blade.

The Inlet surface is positioned 6.75 m upstream of the MEXICO wind turbine, while the Outlet is situated 18 m downstream. The stationary domain has an external radius of 11.25 m. As for the rotational, it has an external radius of 2.7 m and a width of 1.125 m.

**Table 3.** Characteristics of MEXICO wind turbine blades.

| Position (m) | Airfoil | Chord (m) | β (°) | θ (°) |
|---|---|---|---|---|
| 0.225 | Circle | 0.090 | 0 | 0 |
| 0.293 | | 0.090 | 0 | 0 |
| 0.450 | DU 91-W2-250 | 0.240 | 16.4 | 14.1 |
| 0.675 | | 0.207 | 12.1 | 9.8 |
| 0.900 | | 0.178 | 8.3 | 6.0 |
| 1.025 | | 0.166 | 7.1 | 4.8 |
| 1.225 | RISØ A1-21 | 0.150 | 5.5 | 3.2 |
| 1.350 | | 0.142 | 4.8 | 2.5 |
| 1.475 | | 0.134 | 4.0 | 1.7 |
| 1.675 | NACA 64-418 | 0.123 | 3.2 | 0.9 |
| 1.800 | | 0.116 | 2.6 | 0.3 |
| 2.025 | | 0.102 | 1.5 | -0.8 |
| 2.165 | | 0.092 | 0.7 | -1.6 |
| 2.192 | | 0.082 | 0.5 | -1.8 |
| 2.223 | | 0.056 | 0.2 | -2.1 |
| 2.250 | | 0.010 | 0 | -2.3 |

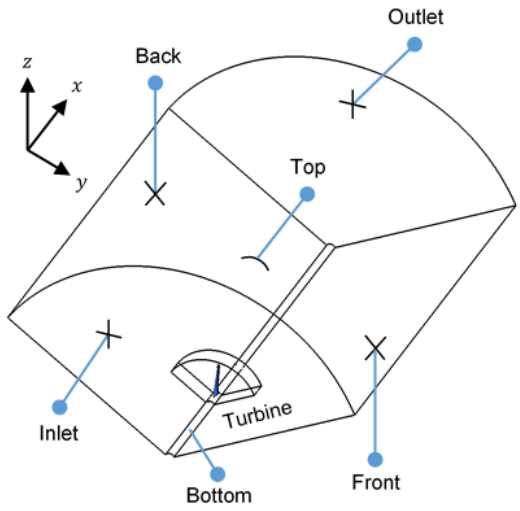


**Fig. 7.** Details of the computational domain for the horizontal axis wind turbine.

The wind turbine blade surface is treated as a wall. The Top face configured as a symmetry plane. The Outlet boundary is assumed to be a pressure outlet, and the Inlet boundary is imposed with different U. The Front and Back faces are treated as periodic. The Bottom surface is set to slip condition.

Four meshes, namely Coarse, Medium, Fine and Extra Fine, are constructed for the grid independence study of the MEXICO wind turbine. These meshes contain 5'149 318, 8'094 168, 14'932 927 and 24'703 452 cells, respectively. The grid independence study evaluates the meshes' results by comparing the torque and thrust for an inlet velocity of 10 m/s. This velocity is chosen because CFD simulations converge faster compared to higher velocities. Additionally, it's noted that y+ value at the blade walls is maintained below 5 for all simulations, including at U = 24 m/s.

#### *2.2.2. Comparative metrics*

For comparing the wind turbine results, the chosen mesh from the grind independence study is utilized. The comparison involves evaluating Cp obtained with the turbulence models at various locations along the blade span: 25%, 35%, 60%, 82% and 92%. The comparison is conducted using the HR and Mean Square Error (MSE) metrics. Unlike NMSE, MSE is suitable for parameters that can take both positive and negative values [38], such as Cp. MSE would be 0 for an ideal model prediction. MSE is defined as follows,

$$MSE = \frac{1}{N}\sum_{i=1}^{N}(P_i - O_i)^2. \quad (9)$$

The threshold values of HR, for the horizontal axis wind turbine are chosen to be similar to those used in the high-rise building study. Note that Ishihara and Qian [39] utilized different HR threshold values for U and TI.

The MSE is a statistical metric employed to assess the precision of a predictive model. It does so by computing the mean of the squared variances between predicted and observed values.

## 3. Results and Discussion

### *3.1. High-Rise Building*

#### 3.1.1. *Grid independence study*

The vertical profiles for U between z = 0.165 and z = 0.29 m, obtained from the Coarse and Fine meshes, are compared for different positions above the building rooftop (V2 to V5), as shown in Figure 8. As depicted in Figure 8, the numerical results of from both meshes exhibit close similarity. Only minor discrepancies are noticeable in positions z = 0.18 to z = 0.20 m at V2 (< 0.3%) and V3 (< 0.4%), and above z = 0.18 m at V4 (< 0.7%) and V5 (< 1%), for both meshes.

Figure 9 illustrated the vertical profiles for k at different axes positions. As observed, minor variations between the results from the Coarse and Fine meshes emerge in positions z = 0.18 to z = 0.22 m at V2, and above z = 0.17 m at V3, V4 and V5. Deviations below 1.13% and 3.25% for U and k, respectively, are found between the Coarse and Fine meshes.

As the numerical results obtained with the Coarse and Fine meshes are closely similar, the Coarse mesh is selected for simulating the subsequent cases. Figure 10 provides details of the Coarse mesh, including the first cell heights adjacent to the building walls, which are set at $5x10^{-5}$, $2x10^{-4}$, $1x10^{-4}$ and $1x10^{-4}$ m for the upstream, downstream, sides and rooftop surfaces, respectively. On the Ground and Sky walls, the first cell heights are $2x10^{-4}$ and $4x10^{-4}$ m. This configuration ensures that y+ remains below 5 on the computational domain walls.

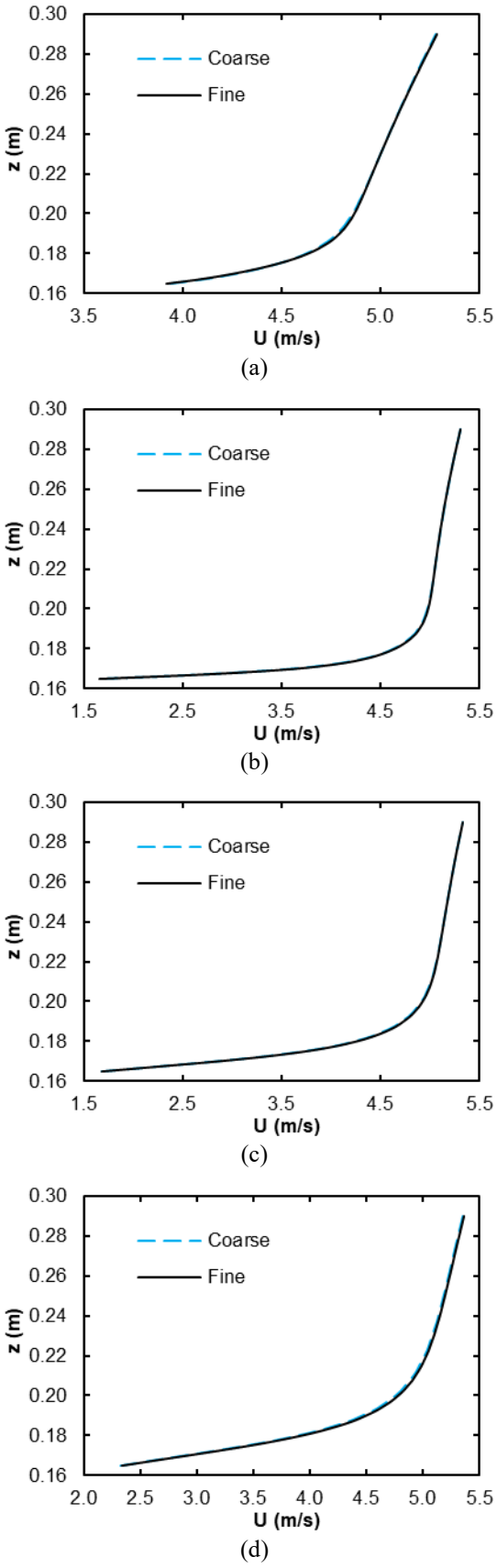


**Fig. 8.** Vertical profiles for U at V2 (a), V3 (b), V4 (c) and V5 (d). Grid independence study.

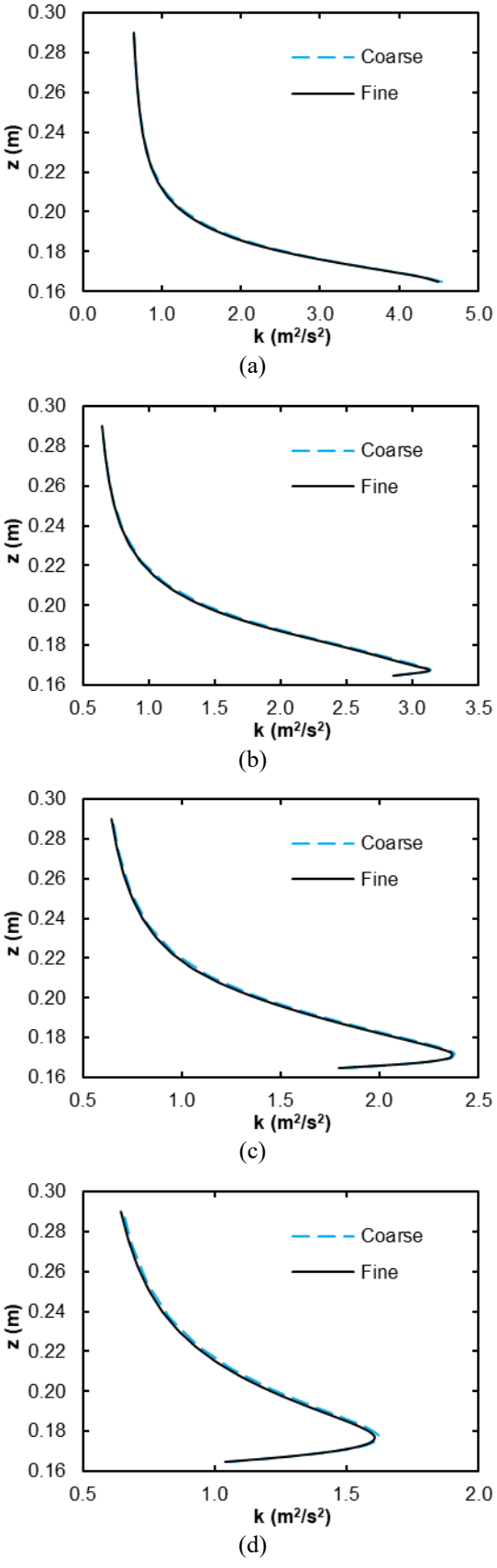


**Fig. 9.** Vertical profiles for k at V2 (a), V3 (b), V4 (c) and V5 (d). Grid independence study.

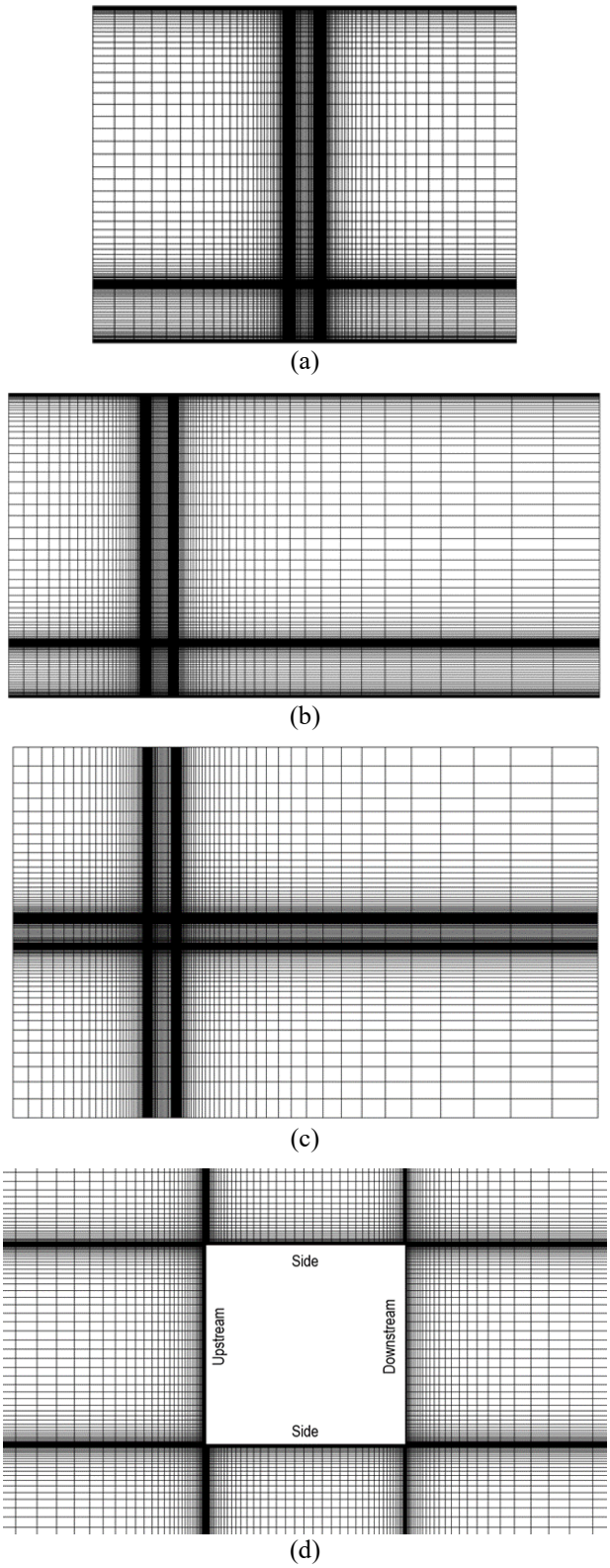


**Fig. 10.** Details of the Coarse mesh. Planes Y-Z (a), Z-X (b), X-Y (c) and around building (d).

### *3.1.2. Comparative metrics*

Vertical profiles for U and k at axes V2 to V5, obtained using the turbulence models, are depicted in **Figure 11** and **Figure 12**. For U, notable differences between the models emerge just above the building rooftop (see Figure 11). Specifically, above the upstream edge of the building (at V2, Figure 11a), the numerical results for U obtained using the Realizable k-ε turbulence model closely align with experimental measurements, showing better agreement than those produced by the SST k-ω model.

As shown in Figure 11b, Figure 11c and Figure 11d, both turbulence models' numerical results exhibit good agreement well with the experiment data at z = 0.22 m and z = 0.28 m, with a maximum deviation of 4.6%. The Realizable k-ε model demonstrates good agreement with the experiment data at z = 0.17 m, except at V4 and V5, where differences of 91.9% are observed.

Overall, the SST k-ω model demonstrates the best agreement with the experiment data for $z \geq 0.19$. Conversely, the SST k-ω model exhibits the worst results for $z < 0.19$ m at all axes.

With regards to vertical profiles for k, the SST k-ω turbulence model exhibits the best agreement with the experiment at V2 (Figure 12a). At V3 (Figure 12b), the results obtained using the SST k-ω model are in good agreement with the experimental measurements from z = 0.22 m to z = 0.28 m (maximum deviation of 11.4%), but it underestimates k at z = 0.17 m, where only the Realizable k-ε model approaches the measurement (error of 11.8%). Noticeable differences between numerical results and experimental measurements emerge just above the building rooftop for all positions, particularly at V4 (Figure 12c) and V5 (Figure 12d). In general, good results are achieved by the SST k-ω model from z = 0.19 m to z = 0.28 m for all positions, while both turbulence models accurately predict k at z = 0.19 at V5 (15% maximum deviation). It is noteworthy that k can not be accurately estimated by the models at z = 0.17 m for all positions.

The HR results for the turbulence models considered in this work are summarized in Table 4. Both models demonstrated good accuracy in capturing U values, with HR > 0.81. However, only the SST k-ω model achieves an HR ≥ 0.66 for k, meeting the minimum criterion for successful HR assessment [15]. In terms of NMSE, the Realizable k-ε model yields the best results for U and k.

Figure 13 and Figure 14 compare U and k, respectively, at the vertical middle section of the computational domain for both turbulence models. In Figure 13, the Realizable k-ε model accurately reproduces the reattachment flow behavior on the building rooftop, whereas the SST k-ω model does not capture this phenomenon. This observation aligns with findings from previous studies [15]. Note that the Realizable k-ε model predicts higher velocities compared to the SST k-ω model. Figure 14 shows the k results obtained with the Realizable k-ε model, which are consistent with the study by Toja-Silva et al. [15]. In their work, k-ε based turbulence models exhibited high k values around the upstream and top faces of the building, similar to the results presented here. However, the results from the SST k-ω model are similar to those reported in [14] for regions near the top and downstream faces of the building. There are differences in the upstream face, where high k values are not observed in the simulations.

This discrepancy could be attributed to the higher mesh refinement used in this study compared to the mesh utilized in [14].

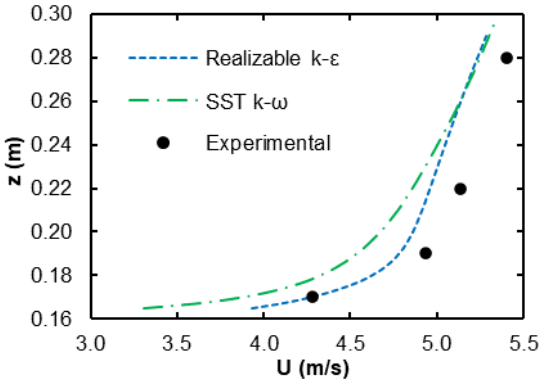


(a)

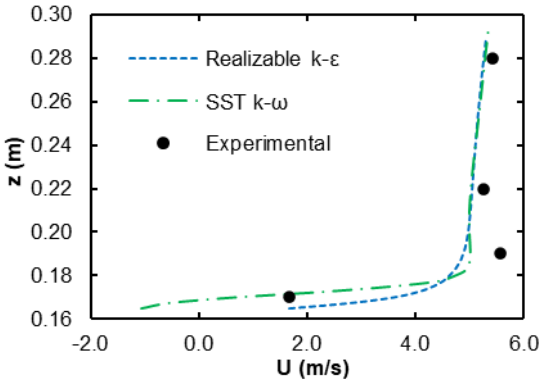


(b)

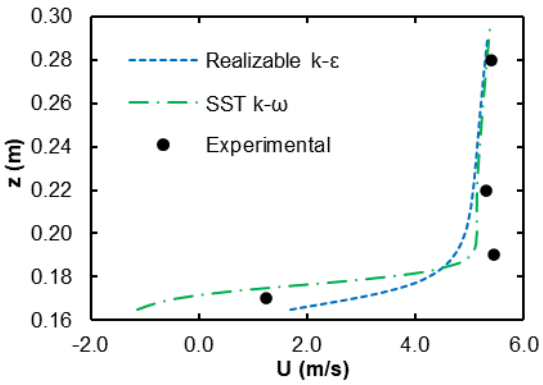


(c)

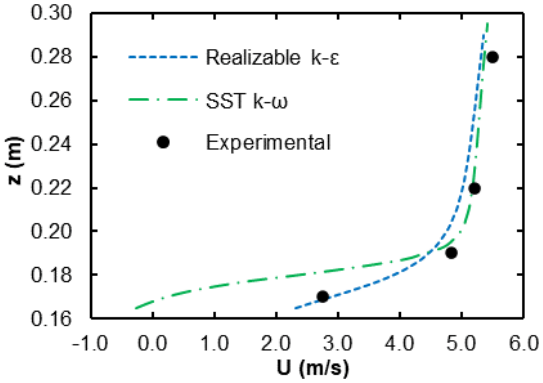


(d)

**Fig. 11.** Vertical profiles for U at V2 (a), V3 (b), V4 (c) and V5 (d). Turbulence models comparison.

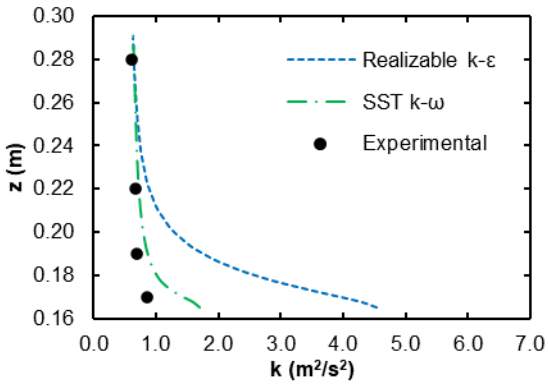


(a)

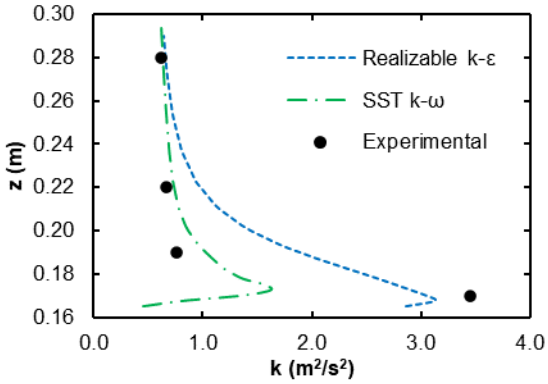


(b)

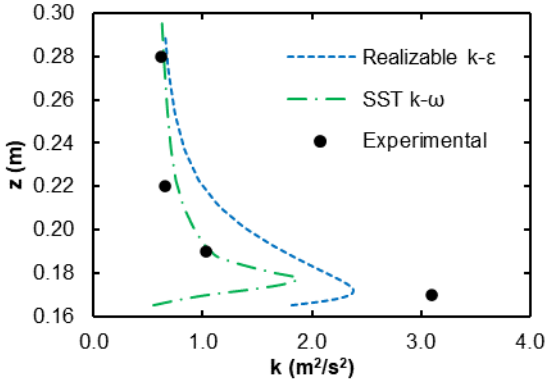


(c)

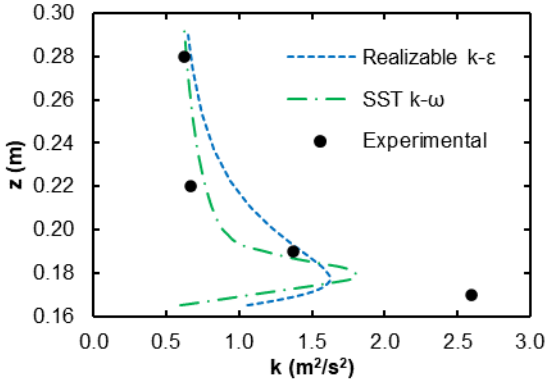


(d)

**Fig. 12.** Vertical profiles for k at V2 (a), V3 (b), V4 (c) and V5 (d). Turbulence models comparison.

**Table 4.** Results of HR and NMSE for the high-rise building

| Turbulence model | $HR_U$ | $HR_k$ | $NMSE_U$ | $NMSE_k$ |
|---|---|---|---|---|
| Realizable k-ε | 0.875 | 0.375 | 0.022 | 0.515 |
| SST k-ω | 0.813 | 0.688 | 0.039 | 0.642 |

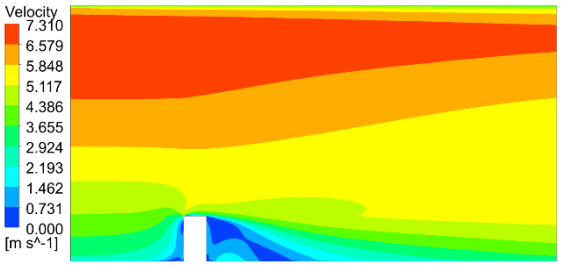


(a)

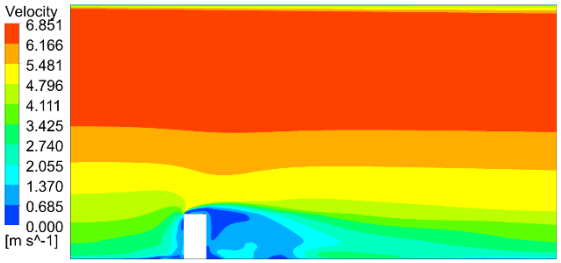


(b)

**Fig. 13.** Contours of U at the vertical middle section of the computational for Realizable k-ε (a) and SST k-ω (b).


(a)

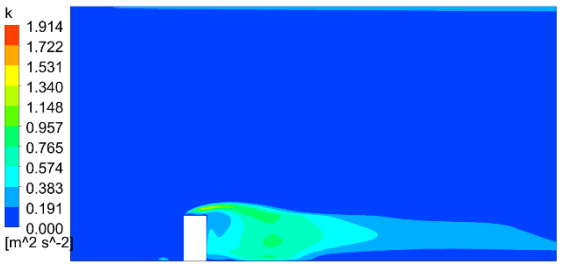


(b)

**Fig. 14.** Contours of k at the vertical middle section of the computational for Realizable k-ε (a) and SST k-ω (b).

### *3.2. Horizontal Axis Wind Turbine*

#### *3.2.1. Grid independence study*

Table 5 and Table 6 present the thrust and torque results for the MEXICO wind turbine at U = 10 m/s, obtained using the Realizable k-ε and SST k-ω models. For the Realizable k-ε model (Table 5), grid independence is achieved with the Fine mesh, as the thrust and torque values differ by only 0.48% and 0.92%, respectively, between the Fine and Extra Fine meshes. In contrast, for the SST k-ω model (Table 6), grid independence is achieved with the Medium mesh. The deviations in thrust and torque between the Medium and Fine meshes are 0.71% and 2.18%, respectively. It's important to note that conducting the grid independence study solely with the SST k-ω turbulence model and using the Medium mesh for subsequent simulations would have been erroneous, as the Realizable k-ε model does not achieve grid independence with that mesh. Therefore, the Fine mesh is chosen for further simulations.

Table 5. Thrust and torque comparison for U = 10 m/s, by using the Realizable k-ε model. Grid independence study.

| Mesh | Thrust (N) | Torque (Nm) |
|---|---|---|
| Coarse | 965 | 18 |
| Medium | 1110 | 69 |
| Fine | 1132 | 80 |
| Extra Fine | 1127 | 79 |

Table 6. Thrust and torque comparison for U = 10 m/s, by using the Realizable k-ω model. Grid independence study.

| Mesh | Thrust (N) | Torque (Nm) |
|---|---|---|
| Coarse | 964 | 37 |
| Medium | 1136 | 87 |
| Fine | 1127 | 85 |
| Extra Fine | 1125 | 84 |

The Fine mesh details are shown in Figure 15. To maintain y+ below 5 on the blade surface, a first cell height of $1x10^{-6}$ m is utilized. Figure 15a demonstrates the utilization of finer elements in perpendicular directions to the blade surfaces. On the blade surface (Figure 15b), there´s a noticeable change in mesh element size, with finer elements near the blade tip (Figure 15c and Figure 15d) and root (Figure 15e), where high gradients are expected. Conversely, coarser elements are distributed across the rest of the surface. Additionally, finer elements are present around the blade surface in normal direction, facilitating the capture of boundary layer physics (Figure 15f).

#### *3.2.2. Comparative metrics*

The numerical results of Cp obtained with the turbulence models are presented at various blade span stations: 25%, 35%, 60%, 82% and 92%. Figure 16 illustrates these results for U = 10 m/s. At this velocity, the Cp results from both turbulence models exhibit close similarity. However, deviations between the results obtained with the SST k-ω and Realizable k-ε models emerge at 25% and 35% blade span for U = 15 m/s. For U = 24 m/s, significant differences between the models are observed, particularly at 60% and 82% blade span and y/c = 0 – 0.4 (airfoil suction side).

Comparing the numerical results and experimental measurements of Cp, it's observed that for U = 24 m/s at 35% of blade span (suction side), the Realizable k-ε model results are closer to the experiment compared to those computed from the SST k-ω model. However, at 25% and 35% blade span (for U = 24 m/s), the SST k-ω model results are closer to the measurements than those obtained by employing the Realizable k-ε model. Conversely, the Realizable k-ε model shows higher accuracy than the SST k-ω model when predicting Cp at 60% and 82% blade span stations.

The HR and MSE computed from Cp for the turbulence models are depicted in Table 7. It's noted that the turbulence models do not exhibit good accuracy in capturing Cp (HR < 0.66). Only the Realizable k-ε model has HR > 0.66 at r/R = 0.60 and r/R = 0.82. Overall, the Realizable k-ε model yields the best HR, while the SST k-ω model demonstrates the best MSE (see Table 8).

**Table 7.** Numerical results of HR and MSE for the horizontal axis wind turbine at different blade span positions.

| **r/R = 0.25** | | | | | | |
|---|---|---|---|---|---|---|
| **Turbulence model** | **U = 10 m/s** | | **U = 15 m/s** | | **U = 24 m/s** | |
| | **HR** | **MSE** | **HR** | **MSE** | **HR** | **MSE** |
| Realizable k-ε | 0.481 | 0.096 | 0.444 | 0.173 | 0.148 | 2.796 |
| SST k-ω | 0.481 | 0.097 | 0.407 | 0.221 | 0.259 | 2.313 |
| **r/R = 0.35** | | | | | | |
| **Turbulence model** | **U = 10 m/s** | | **U = 15 m/s** | | **U = 24 m/s** | |
| | **HR** | **MSE** | **HR** | **MSE** | **HR** | **MSE** |
| Realizable k-ε | 0.462 | 0.226 | 0.500 | 0.238 | 0.370 | 1.338 |
| SST k-ω | 0.423 | 0.228 | 0.500 | 0.259 | 0.481 | 0.938 |
| **r/R = 0.60** | | | | | | |
| **Turbulence model** | **U = 10 m/s** | | **U = 15 m/s** | | **U = 24 m/s** | |
| | **HR** | **MSE** | **HR** | **MSE** | **HR** | **MSE** |
| Realizable k-ε | 0.417 | 0.034 | 0.500 | 0.088 | 0.708 | 0.329 |
| SST k-ω | 0.417 | 0.035 | 0.458 | 0.110 | 0.417 | 0.066 |
| **r/R = 0.82** | | | | | | |
| **Turbulence model** | **U = 10 m/s** | | **U = 15 m/s** | | **U = 24 m/s** | |
| | **HR** | **MSE** | **HR** | **MSE** | **HR** | **MSE** |
| Realizable k-ε | 0.500 | 0.033 | 0.625 | 0.055 | 0.750 | 0.282 |
| SST k-ω | 0.542 | 0.035 | 0.625 | 0.063 | 0.250 | 0.435 |
| **r/R = 0.92** | | | | | | |
| **Turbulence model** | **U = 10 m/s** | | **U = 15 m/s** | | **U = 24 m/s** | |
| | **HR** | **MSE** | **HR** | **MSE** | **HR** | **MSE** |
| Realizable k-ε | 0.360 | 0.024 | 0.600 | 0.054 | 0.480 | 0.646 |
| SST k-ω | 0.400 | 0.025 | 0.600 | 0.061 | 0.440 | 0.447 |

**Table 8.** Summarizing the numerical results for the horizontal axis wind turbine.

| **Turbulence model** | **HR** | **MSE** |
|---|---|---|
| Realizable k-ε | 0.485 | 0.445 |
| SST k-ω | 0.451 | 0.370 |

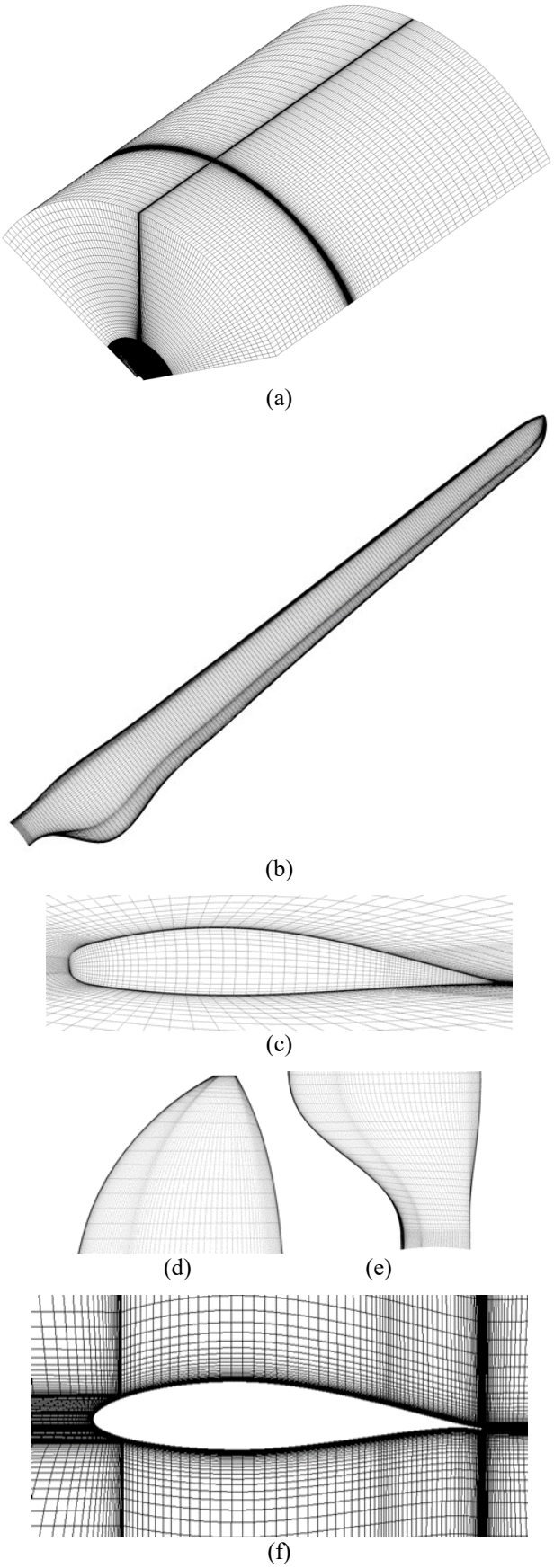


**Fig. 15.** Details of the Fine mesh. Isometric view of the domain (a), blade (b), plan view of the tip (c), tip of the blade (d), root of the blade (e), and boundary layer around blade surface (f).

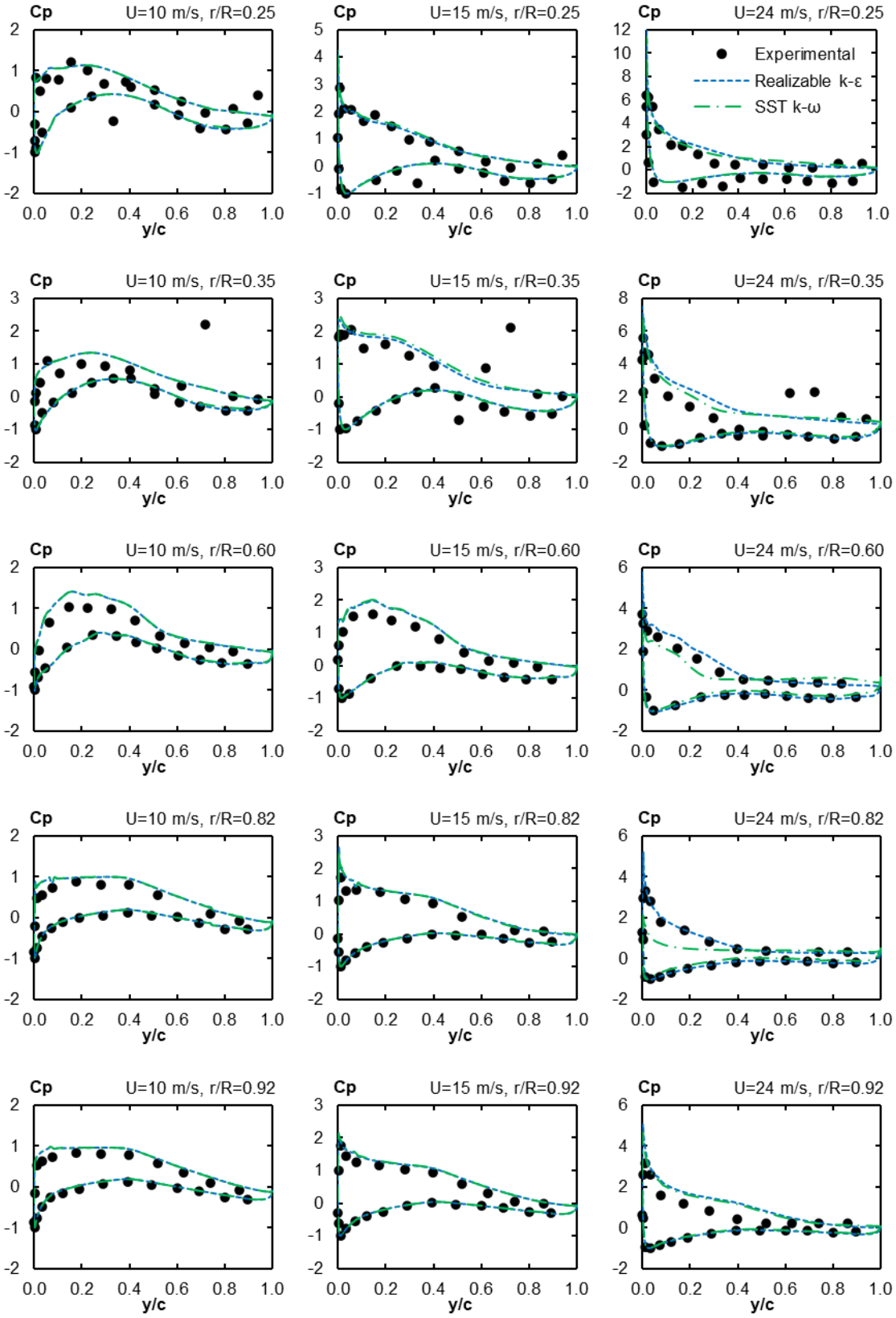


**Fig. 16.** Cp distributions at 25%, 35%, 60%, 82% and 92% blade span stations for U = 10, 15 and 24 m/s.

Figure 17 shows the contours of pressure around different blade span stations (25%, 35%, 60%, 82% and 92%) for the Realizable k-ε and SST k-ω turbulence models at U = 10 m/s. While the minimum and maximum pressure values obtained by both models are similar, the distribution of this parameter around the blade span positions is clearly different. Specifically, the Realizable k-ε model yields higher pressure values (5 664 Pa) compared to the SST k-ω model (5 624 Pa).

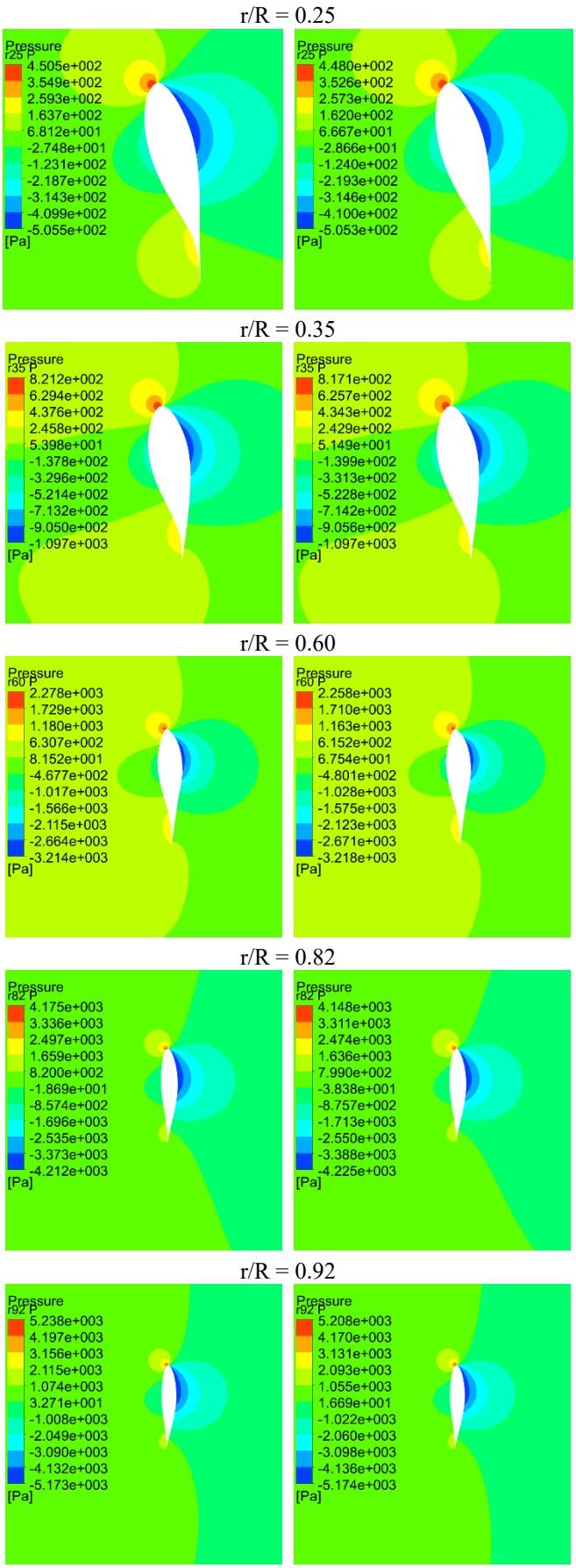


**Fig. 17.** Contours of pressure at 25%, 35%, 60%, 82% and 92% blade span stations, for the Realizable k-ε (left) and SST k-ω (right) models, by using U = 10 m/s.

Note that the incorporation of renewable energies into power systems is promoted by governments to mitigate greenhouse gas emissions produced from fossil fuel combustion [40] [41]. Therefore, it is important to continue researching topics related to urban wind energy, such as forecasting wind speeds using machine learning models [42] [43] and hybrid photovoltaic-wind systems [44].

## 4. Conclusion

This paper aimed to validate the numerical results of both a high-rise building and a horizontal axis wind turbine using the Realizable k-ε and SST k-ω turbulence models. While several previous CFD studies have individually examined either high-rise buildings or horizontal axis wind turbines, none have comprehensively validated both models within the same study.

Accordingly, detailed models of the high-rise building and horizontal axis wind turbine models were described, referencing the Case A (Architectural Institute of Japan) and the MEXICO project (Large Scale Low Speed Facility), respectively. Grid independence studies were conducted using meshes of varying refinement levels. The obtained numerical results were then compared with experimental measurements using comparative metrics such as HR, NMSE and MSE, focusing on parameters including U, k and Cp.

Overall, the numerical results obtained with the turbulence models demonstrated good agreement with the experimental measurements. Specifically, the Realizable k-ε model performed better in predicting the flow pattern on the building rooftop, achieving HR > 0.813 and 0.375 for U and k, respectively, along with the best NMSE of 0.022. On the other hand, the SST k-ω outperformed the Realizable k-ε model in simulating the horizontal axis wind turbine, with the best HR of 0.485 and a better MSE of 0.37. These findings suggest that for single simulations of the high-rise building and horizontal axis wind turbine, the Realizable k-ε and SST k-ω models should be employed, respectively. For simulations involving both models, such as urban wind energy applications, the SST k-ω model is recommended due to its superior ability to predict pressure on wind turbine blade surfaces and capture wind flow behavior above building rooftops, where small horizontal axis wind turbines are commonly located.

### Acknowledgements

Christian V. Rodriguez gratefully acknowledges the financial support provided by the Consejo Nacional de Ciencia, Tecnología e Innovación (CONCYTEC), which enabled the development of this research.

### Author Contributions

Christian V. Rodriguez was responsible for the methodology, formal analysis, software development, and original draft preparation. Alberto Ríos was responsible for the conceptualization and supervision, and contributed to the review and editing of the manuscript. Jaime E. Luyo

contributed to the review and editing of the manuscript. All authors have read and agreed to the published version of the manuscript.

**Conflict of Interest**

The authors declare that there are no conflicts of interest regarding the research, authorship, and publication of this article.

**References**

[1] T. F. Ishugah, Y. Li, R. Z. Wang, and J. K. Kiplagat, "Advances in wind energy resource exploitation in urban environment: A review," Renewable and Sustainable Energy Reviews, vol. 37, pp. 613–626, 2014. doi: 10.1016/j.rser.2014.05.053.

[2] E. Arteaga-López, C. Ángeles-Camacho, and F. Bañuelos-Ruedas, "Advanced methodology for feasibility studies on building-mounted wind turbines installation in urban environment: Applying CFD analysis," Energy, vol. 167, pp. 181–188, 2019. doi: 10.1016/j.energy.2018.10.191.

[3] F. Toja-Silva, C. Peralta, O. Lopez-Garcia, J. Navarro, and I. Cruz, "On roof geometry for urban wind energy exploitation in high-rise buildings," Computation, vol. 3, no. 2, pp. 299–325, 2015. doi: 10.3390/computation3020299.

[4] A. Ricci, I. Kalkman, B. Blocken, M. Burlando, and M. P. Repetto, "Impact of turbulence models and roughness height in 3D steady RANS simulations of wind flow in an urban environment," Building and Environment, vol. 171, p. 106617, 2020. doi: 10.1016/j.buildenv.2019.106617.

[5] R. Yoshie, et al., "Cooperative project for CFD prediction of pedestrian wind environment in the Architectural Institute of Japan," Journal of Wind Engineering and Industrial Aerodynamics, vol. 95, no. 9–11, pp. 1551–1578, 2007. doi: 10.1016/j.jweia.2007.02.023.

[6] K. K. Vranešević, G. Vita, S. P. A. Bordas, and A. Š. Glumac, "Furthering knowledge on the flow pattern around high-rise buildings: LES investigation of the wind energy potential," Journal of Wind Engineering and Industrial Aerodynamics, vol. 226, July 2022. doi: 10.1016/j.jweia.2022.105029.

[7] S. Masoumi-Verki, P. Gholamalipour, F. Haghighat, and U. Eicker, "Embedded LES of thermal stratification effects on the airflow and concentration fields around an isolated high-rise building: Spectral and POD analyses," Building and Environment, vol. 206, Dec. 2021. doi: 10.1016/j.buildenv.2021.108388.

[8] Y. H. Juan, C. Y. Wen, W. Y. Chen, and A. S. Yang, "Numerical assessments of wind power potential and installation arrangements in realistic highly urbanized areas," Renewable and Sustainable Energy Reviews, vol. 135, p. 110165, 2021. doi: 10.1016/j.rser.2020.110165.

[9] Y. H. Juan, A. Rezaeiha, H. Montazeri, B. Blocken, C. Y. Wen, and A. S. Yang, "CFD assessment of wind energy potential for generic high-rise buildings in close proximity: Impact of building arrangement and height," Applied Energy, vol. 321, Sep. 2022. doi: 10.1016/j.apenergy.2022.119328.

[10] Y. Tominaga, A. Mochida, S. Murakami, and S. Sawaki, "Comparison of various revised k-ε models and LES applied to flow around a high-rise building model with 1:1:2 shape placed within the surface boundary layer," Journal of Wind Engineering and Industrial Aerodynamics, vol. 96, no. 4, pp. 389–411, 2008. doi: 10.1016/j.jweia.2008.01.004.

[11] Architectural Institute of Japan, *Guidebook for CFD Predictions of Urban Wind Environment*, [Online]. Available: https://www.aij.or.jp/jpn/publish/cfdguide/index_e.htm. Accessed: Oct. 26, 2021.

[12] P. Gousseau, B. Blocken, and G. J. F. Van Heijst, "Quality assessment of Large-Eddy Simulation of wind flow around a high-rise building: Validation and solution verification," Computer & Fluids, vol. 79, pp. 120–133, 2013. doi: 10.1016/j.compfluid.2013.03.006.

[13] J. Liu and J. Niu, "CFD simulation of the wind environment around an isolated high-rise building: An evaluation of SRANS, LES and DES models," Building and Environment, vol. 96, pp. 91–106, 2016. doi: 10.1016/j.buildenv.2015.11.007.

[14] Y. Tominaga, "Flow around a high-rise building using steady and unsteady RANS CFD: Effect of large-scale fluctuations on the velocity statistics," Journal of Wind Engineering and Industrial Aerodynamics, vol. 142, pp. 93–103, 2015. doi: 10.1016/j.jweia.2015.03.013.

[15] F. Toja-Silva, C. Peralta, O. Lopez-Garcia, J. Navarro, and I. Cruz, "Roof region dependent wind potential assessment with different RANS turbulence models," Journal of Wind Engineering and Industrial Aerodynamics, vol. 142, pp. 258–271, 2015. doi: 10.1016/j.jweia.2015.04.012.

[16] M. Shirzadi, P. A. Mirzaei, and M. Naghashzadegan, "Improvement of k-epsilon turbulence model for CFD simulation of atmospheric boundary layer around a high-rise building using stochastic optimization and Monte Carlo sampling technique," Journal of Wind Engineering and Industrial Aerodynamics, vol. 171, pp. 366–379, 2017. doi: 10.1016/j.jweia.2017.10.005.

[17] M. Xiong, B. Chen, H. Zhang, and Y. Qian, "Study on accuracy of CFD simulations of wind environment around high-rise buildings: A comparative study of k-ε turbulence models based on polyhedral meshes and wind tunnel experiments," Applied Sciences, vol. 12, no. 14, July 2022. doi: 10.3390/app12147105.

[18] N. N. Sørensen, J. A. Michelsen, and S. Schreck, "Navier-Stokes predictions of the NREL phase VI rotor in the NASA Ames 80-by-120 wind tunnel," ASME 2002

Wind Energy Symposium, pp. 94–105, 2002. doi: 10.1002/we.64.

[19] B. Kamalov, S. Batay, D. Zhangaskhanov, Y. Zhao, and E. Y. K. Ng, "Arbitrary hybrid turbulence modeling approach for high-fidelity NREL phase VI wind turbine CFD simulation," Fluids, vol. 7, no. 7, July 2022. doi: 10.3390/fluids7070236.

[20] M. Z. Akhter, A. R. Ali, H. K. Jawahar, F. K. Omar, and E. Elnajjar, "Performance enhancement of small-scale wind turbine featuring morphing blades," Energy, vol. 278, Sep. 2023. doi: 10.1016/j.energy.2023.127772.

[21] M. A. Elfarra, N. Sezer-Uzol, and I. S. Akmandor, "NREL VI rotor blade: Numerical investigation and winglet design and optimization using CFD," Wind Energy, vol. 17, no. 4, pp. 605–626, 2014.

[22] E. S. Abdelghany, H. H. Sarhan, R. Alahmadi, and M. B. Farghaly, "Study the effect of winglet height length on the aerodynamic performance of horizontal axis wind turbines using computational investigation," Energies, vol. 16, no. 13, July 2023.

[23] A. M. AbdelSalam and V. Ramalingam, "Wake prediction of horizontal-axis wind turbine using full-rotor modeling," Journal of Wind Engineering and Industrial Aerodynamics, vol. 124, pp. 7–19, 2014.

[24] J. G. Schepers and H. Snel, *Model Experiments in Controlled Conditions*, 2007.

[25] A. Bechmann, N. N. Sørensen, and F. Zahle, "CFD simulations of the MEXICO rotor," Wind Energy, vol. 14, no. 5, pp. 677–689, July 2011. doi: 10.1002/we.450.

[26] P. G. Regodeseves and C. S. Morros, "Unsteady numerical investigation of the full geometry of a horizontal axis wind turbine: Flow through the rotor and wake," Energy, vol. 202, p. 117674, 2020.

[27] R. V. Rodrigues and C. Lengsfeld, "Development of a computational system to improve wind farm layout, Part I: Model validation and near wake analysis," Energies, vol. 12, no. 5, 2019.

[28] I. Herraez, W. Medjroubi, B. Stoevesandt, and J. Peinke, "Aerodynamic simulation of the MEXICO rotor," Journal of Physics: Conference Series, vol. 555, no. 1, 2014.

[29] S. Amini, M. R. Golzarian, E. Mahmoodi, A. Jeromin, and M. H. Abbaspour-Fard, "Numerical simulation of the Mexico wind turbine using the actuator disk model along with the 3D correction of aerodynamic coefficients in OpenFOAM," Renewable Energy, vol. 163, pp. 2029–2036, 2021. doi: 10.1016/j.renene.2020.10.120.

[30] P. A. C. Rocha, H. H. B. Rocha, F. O. M. Carneiro, M. E. V. da Silva, and C. F. de Andrade, "A case study on the calibration of the k-ω SST (shear stress transport) turbulence model for small scale wind turbines designed with cambered and symmetrical airfoils," Energy, vol. 97, pp. 144–150, 2016.

[31] P. Larin, M. Paraschivoiu, and C. Aygun, "CFD based synergistic analysis of wind turbines for roof mounted integration," Journal of Wind Engineering and Industrial Aerodynamics, vol. 156, pp. 1–13, 2016.

[32] A. Krishnan and M. Paraschivoiu, "3D analysis of building mounted VAWT with diffuser shaped shroud," Sustainable Cities and Society, vol. 27, pp. 160–166, 2016.

[33] J. Thé and H. Yu, "A critical review on the simulations of wind turbine aerodynamics focusing on hybrid RANS-LES methods," Energy, vol. 138, pp. 257–289, 2017. doi: 10.1016/j.energy.2017.07.028.

[34] T.-H. Shih, W. W. Liou, A. Shabbir, Z. Yang, and J. Zhu, "A new k-ϵ eddy viscosity model for high Reynolds number turbulent flows," Computer & Fluids, vol. 24, no. 3, pp. 227–238, Mar. 1995.

[35] F. R. Menter, "Two-equation eddy-viscosity turbulence models for engineering applications," AIAA Journal, vol. 32, no. 8, pp. 1598–1605, 1994.

[36] Y. Cheng, F. S. Lien, E. Yee, and R. Sinclair, "A comparison of large eddy simulations with a standard k-ε Reynolds-averaged Navier-Stokes model for the prediction of a fully developed turbulent flow over a matrix of cubes," Journal of Wind Engineering and Industrial Aerodynamics, vol. 91, no. 11, pp. 1301–1328, 2003. doi: 10.1016/j.jweia.2003.08.001.

[37] Y. Meng and K. Hibi, "Turbulent measurements of the flow field around a high-rise building," Wind Engineers, JAWE, vol. 1998, no. 76, pp. 55–64, 1998.

[38] M. Schatzmann, H. Olesen, and J. Franke, "Cost 732 model evaluation case studies: Approach and results," COST Action, no. 732, p. 732, 2010.

[39] T. Ishihara and G. W. Qian, "A new Gaussian-based analytical wake model for wind turbines considering ambient turbulence intensities and thrust coefficient effects," Journal of Wind Engineering and Industrial Aerodynamics, vol. 177, pp. 275–292, June 2018.

[40] S. Ozdemir, U. S. Selamogullari, and O. Elma, "Analyzing the effect of inverter efficiency improvement in wind turbine systems," 3rd International Conference on Renewable Energy Research and Application (ICRERA), pp. 572–575, 2014.

[41] M. Caruso, A. Di Tommaso, F. Genduso, R. Miceli, G. Ricco Galluzzo, C. Spataro, and F. Viola, "Experimental characterization of a wind generator prototype for sustainable small wind farms," 2016 IEEE International Conference on Renewable Energy Research and Application (ICRERA), pp. 1202–1206, 2017.

[42] R. Al-Hajj, M. M. Fouad, and E. Mabrouk, "Short-term wind energy forecasting with independent daytime/nighttime machine learning models," 2022 IEEE 12th International Conference on Renewable Energy Research and Applications (ICRERA), pp. 186–191, Sep. 2022.

[43] R. Al-Hajj, M. M. Fouad, A. A. Smieee, and E. Mabrouk, "Ultra-short-term forecasting of wind speed using lightweight features and machine learning models," 2023 IEEE 12th International Conference on Renewable Energy Research and Applications (ICRERA), pp. 93–97, Aug. 2023.

[44] C. Serir, D. Rekioua, S. Bensmail, A. Belkaid, K. Tadjine, S. Hadji, and I. Colak, "Electrification of a load by a hybrid photovoltaic-wind system with battery storage," 2022 IEEE 11th International Conference on Renewable Energy Research and Application (ICRERA), pp. 571–575, Sep. 2022.